Plant Physiology®

Plant Physiology, 2025, **197**, kiae617
https://doi.org/10.1093/plphys/kiae617
Advance access publication 19 November 2024
Research Article

Cyclic and pseudo-cyclic electron pathways play antagonistic roles during nitrogen deficiency in *Chlamydomonas reinhardtii*

Ousmane Dao,[1,*] Adrien Burlacot,[2,3] Felix Buchert,[4] Marie Bertrand,[1] Pascaline Auroy,[1] Carolyne Stoffel,[2] Sai Kiran Madireddi,[2] Jacob Irby,[2] Michael Hippler,[4,5] Gilles Peltier,[1] Yonghua Li-Beisson[1,*]

[1]Aix Marseille University, CEA, CNRS, Institute of Biosciences and Biotechnology of Aix Marseille, BIAM, CEA Cadarache, Saint Paul-Lez-Durance, 13118, France
[2]Department of Plant Biology, The Carnegie Institution for Science, Stanford, CA 94305, USA
[3]Department of Biology, Stanford University, Stanford, CA 94305, USA
[4]Institute of Plant Biology and Biotechnology, University of Münster, Münster 48143, Germany
[5]Institute of Plant Science and Resources, Okayama University, Kurashiki 710-0046, Japan
*Author for correspondence: yonghua.li@cea.fr (Y.L.-B.), ousmanedao17@yahoo.fr (O.D.)
The author responsible for distribution of materials integral to the findings presented in this article in accordance with the policy described in the Instructions for Authors (https://academic.oup.com/plphys/pages/General-Instructions) is Yonghua Li-Beisson (yonghua.li@cea.fr).

Abstract

Nitrogen (N) scarcity frequently constrains global biomass productivity. N deficiency halts cell division, downregulates photosynthetic electron transfer (PET), and enhances carbon storage. However, the molecular mechanism downregulating photosynthesis during N deficiency and its relationship with carbon storage are not fully understood. Proton gradient regulator-like 1 (PGRL1) controlling cyclic electron flow (CEF) and flavodiiron proteins (FLV) involved in pseudo-CEF (PCEF) are major players in the acclimation of photosynthesis. To determine the role of PGRL1 or FLV in photosynthesis under N deficiency, we measured PET, oxygen gas exchange, and carbon storage in *Chlamydomonas reinhardtii pgrl1* and *flvB* knockout mutants. Under N deficiency, *pgrl1* maintained higher net photosynthesis and O_2 photoreduction rates and higher levels of cytochrome b_6f and PSI compared with the control and *flvB*. The photosynthetic activity of *flvB* and *pgrl1 flvB* double mutants decreased in response to N deficiency, similar to the control strains. Furthermore, the preservation of photosynthetic activity in *pgrl1* was accompanied by an increased accumulation of triacylglycerol in certain genetic backgrounds but not all, highlighting the importance of gene–environment interaction in determining traits such as oil content. Our results suggest that in the absence of PGRL1-controlled CEF, FLV-mediated PCEF maintains net photosynthesis at a high level and that CEF and PCEF play antagonistic roles during N deficiency. This study further illustrate how a strain's nutrient status and genetic makeup can affect the regulation of photosynthetic energy conversion in relation to carbon storage and provide additional strategies for improving lipid productivity in algae.

Introduction

Nitrogen (N) deficiency is one of the most harsh environmental situation that constrains global primary biomass productivity in all ecosystems (Vitousek and Howarth 1991; LeBauer and Treseder 2008; Du et al. 2020). Under N deficiency, cell division stops and photosynthetic CO_2 assimilation is downregulated, the carbon and energy being used to synthesize starch and triacylglycerols (TAGs) (Siaut et al. 2011; Schmollinger et al. 2014; Juergens et al. 2015; Schulz-Raffelt et al. 2016). The downregulation of photosynthetic electron transfer (PET) reactions, together with a rerouting of the excess reducing power toward carbon storage, prevents the overproduction of reactive oxygen species, thus ensuring cell fitness (Zhang et al. 2013; Park et al. 2015; Gargouri et al. 2017; Du et al. 2018; Tran et al. 2019).

Due to the variability in their natural habitat, microalgae must constantly adjust the photosynthetic conversion of energy to match the metabolic demand and have therefore developed a set of regulatory mechanisms to fine-tune electron transfer reactions. During photosynthetic linear electron flow (LEF), electrons generated by water splitting are used to reduce $NADP^+$ to NADPH, and the electron flow generates an electrochemical proton gradient across the thylakoid membrane, which can be used to produce ATP (Allen 2003). The balance of ATP and NADPH is essential for optimal CO_2 capture and metabolism to which cyclic electron flow (CEF) and pseudo-cyclic electron flow (PCEF) play a critical role (Dang et al. 2014; Bailleul et al. 2015; Burlacot et al. 2019; Saroussi et al. 2019; Peltier et al. 2024). Two pathways of CEF around the photosystem I (PSI) have been described in the green microalga *Chlamydomonas reinhardtii* (*Chlamydomonas* hereafter), one involving the type II NADPH dehydrogenase (NDA2) (Desplats et al. 2009), and the other being controlled by the proton gradient regulator 5 (PGR5)/PGR-like 1 (PGRL1) proteins (Tolleter et al. 2011).

Recent work in *Chlamydomonas* provided evidence that PGR5 and PGRL1 are involved in CEF (Petroutsos et al. 2009; Tolleter et al. 2011; Johnson et al. 2014). Hereby, PGR5 is required for efficient stromal electron intake into the cytochrome b_6f (Cyt b_6f) complex (Buchert et al. 2020). Its deletion strongly disturbs the Mitchellian Q cycle (Buchert et al. 2020). Also, deletion of PGRL1 impacts CEF in *Chlamydomonas* (Petroutsos et al. 2009; Tolleter et al. 2011). Despite the fact that PGRL1 has been implicated in plastoquinone (PQ) reduction during CEF (Hertle et al. 2013), it appears that

Received July 12, 2024. Accepted October 7, 2024.

PGRL1 is rather important for PGR5 expression and protein stability, as in the absence of PGRL1, PGR5 is strongly diminished, mimicking PGR5-dependent phenotypes (DalCorso et al. 2008; Petroutsos et al. 2009; Rühle et al. 2021).

Both CEF pathways reduce the PQ pool by using either NADPH or ferredoxin (Fd) as electron donor, respectively (Tagawa et al. 1963; Desplats et al. 2009; Hertle et al. 2013). CEF has been shown to contribute to the acidification of thylakoid lumen by generating an extra proton motive force (*pmf*) in addition to the one produced by LEF (Munekage et al. 2002; Desplats et al. 2009; Tolleter et al. 2011; Saroussi et al. 2016). PCEF mediated by flavodiiron proteins (FLVs), by transferring electrons toward O_2 at the acceptor side of PSI, also contributes to the establishment of the *pmf* and therefore to the lumen acidification (Gerotto et al. 2016; Chaux et al. 2017a; Burlacot et al. 2022). The *pmf* is used to either (1) produce ATP (Allen 2002), (2) trigger light energy quenching via a low lumenal pH (Peers et al. 2009; Bonente et al. 2011; Erickson et al. 2015), (3) convert HCO_3^- into CO_2 thanks to carbonic anhydrase in the lumen (Burlacot et al. 2022), or (4) repress electron transfer at the level the Cyt b_6f complex through the photosynthetic control triggered by the low lumenal pH (Stiehl and Witt 1969; Foyer et al. 1990; Munekage et al. 2001; Munekage et al. 2002; Malone et al. 2021). Both CEF and PCEF have been shown to be critical under various conditions of light, CO_2 availability or sulfur deficiency by playing a synergistic role (Dang et al. 2014; Jokel et al. 2015; Chaux et al. 2017a; Jokel et al. 2018; Burlacot et al. 2022).

Despite the importance of CEF and PCEF in response to dynamic environments, little is known about their role during N deficiency. The role of NDA2-involved CEF have been recently addressed during CO_2-limiting photoautotrophic N deficiency and the knockdown of NDA2 was shown to impair the establishment of nonphotochemical quenching (Saroussi et al. 2016). The role of PGRL1/PGR5-controlled CEF has been investigated under mixotrophic N deficiency and the lack of PGRL1 was shown to decrease the rate of CEF and a lower TAG production (Chen et al. 2015). However, the role of PGRL1 during photoautotrophic N deficiency and the possible bioenergetic interactions between carbon/energy sinks (TAG and starch) and CEF or PCEF pathways that generate ATP has not yet been explored so far. Considering that massive carbon storage occurs under N deficiency (Siaut et al. 2011), the bioenergetics governing the associated metabolic remodeling during N deficiency are likely critical. Fully understanding of photosynthesis regulatory pathways and how they affect carbon storage is needed toward engineering photosynthesis and carbon storage in conditions of nutrient deficiency.

Here, we evaluated the contribution of PGRL1/PGR5-controlled CEF in the regulation of photosynthesis during N deficiency and evaluate its metabolic consequences on carbon storage in *Chlamydomonas* cells grown in photoautotrophic conditions under nonlimiting CO_2 concentrations (using 1% CO_2-enriched air), conditions which favor the accumulation of carbon reserves (Schulz-Raffelt et al. 2016; Kong et al. 2018; Wu et al. 2019). By monitoring photosynthetic activity based on chlorophyll fluorescence and O_2 exchange rate measurements, we observed high net photosynthetic activity in PGRL1-deficient strains under N deficiency compared with the control strains. Furthermore, the lack of PGRL1 resulted in an overaccumulation of TAGs in some genetic backgrounds but not in others. Those effects being suppressed in double mutants deficient in both PGRL1 and FLVB. We conclude that FLVs, by maintaining a strong PCEF activity in the *pgrl1* mutants, catalyze high photosynthetic rates. Finally, we discuss how modulating photosynthetic electron flow could constitute an efficient strategy to improve photosynthesis and eventually offer additional strategies to boost further TAG production under N deficiency.

Results

Photosynthetic activity sustained longer in *pgrl1* under N deficiency

To assess the role of the PGRL1/PGR5-controlled CEF in the regulation of photosynthesis during photoautotrophic N deficiency, we simultaneously monitored chlorophyll fluorescence and O_2 exchange following a dark–light–dark transition in N-replete and N-deprived cells. We compared the photosynthesis efficiency of a PGRL1-deficient strain ($pgrl1_{137AH}$) with its control wild-type strain (137AH) and a complemented line (Tolleter et al. 2011) (Fig. 1; Supplementary Figs. S1 and S2). Under N-replete conditions, both chlorophyll fluorescence and O_2 exchange patterns were mostly similar in $pgrl1_{137AH}$ and control cells (Fig. 1, A, C, E, and F; Supplementary Fig. S1, B and C). Under N deficiency, the PSII operating yield measured after 22, 28, 46, and 50 h decreased in all strains but was maintained at a higher level in $pgrl1_{137AH}$ (Supplementary Fig. S1C). After 48 h of N deficiency, the PSII operating yield measured in the light decreased by about 75% in the wild-type and only by 35% in $pgrl1_{137AH}$ (Fig. 1, A, B, and E; Supplementary Fig. S1E). Conversely, $pgrl1_{137AH}$ showed twice higher net O_2 evolution and light-dependent O_2 uptake when compared with the wild-type (Fig. 1, D and F). As previously reported (Peltier and Schmidt 1991; Schmollinger et al. 2014), the dark O_2 consumption rate was stimulated in the 137AH wild-type strain during N deficiency, this effect being reduced in $pgrl1_{137AH}$ (Fig. 1D; Supplementary Fig. S2B). By using $pgrl1_{137AH}$ complemented line *pgrl1*::*PGRL1*-2 (Tolleter et al. 2011), we noticed a full recovery of all the observed phenotypes (Supplementary Fig. S1, E to G; Supplementary Figs. S1 and S2). To further strengthen the phenotype–genotype relationship, we generated 3 additional $pgrl1_{CC125}$ mutants in the CC125 wild-type genetic background using CRISPR–Cas9 (Supplementary Figs. S3 to S4). We have observed 45% to 30% higher PSII operating yield in the 3 $pgrl1_{CC125}$ mutants ($pgrl1_{CC125}$-86, $pgrl1_{CC125}$-60, and $pgrl1_{CC125}$-75) after 24 h of N deficiency compared with wild-type CC125, this effect being weaker after 48 h of N deficiency (Supplementary Fig. S3). We then measured O_2 exchange rate after 24 h of N deficiency and reported a 30% higher net O_2 evolution and about twice higher gross O_2 production and uptake in $pgrl1_{CC125}$-86 compared with the wild-type CC125 (Supplementary Fig. S3, D and E). The higher O_2 consumption under N deficiency in the dark-adapted 137AH strain from Fig. 1D was independent of PGRL1 in the CC125 background (Supplementary Fig. S3, D and E). Thus, photosynthetic activity was retained longer in PGRL1-deficient strains during N deficiency, with the magnitude and the duration of this retention being dependent on genetic background. We conclude from those results that PGRL1-controlled CEF contributes to repressing the PET reactions under photoautotrophic N deficiency.

The PGRL1 modulates the PSI donor and acceptor side during N deficiency

The PGRL1/PGR5-controlled CEF is a determinant of the downstream PSI electron fate which prompted us to monitor P700, the primary PSI donor after 24 h of N deficiency when *pgrl1* mutants from both genetic backgrounds showed higher photosynthetic activity compared with their respective wild-types (Fig. 2; Supplementary Fig. S4). P700 forms 3 populations and only the first 2 are photo-oxidizable: (1) PSI donor shortage generates

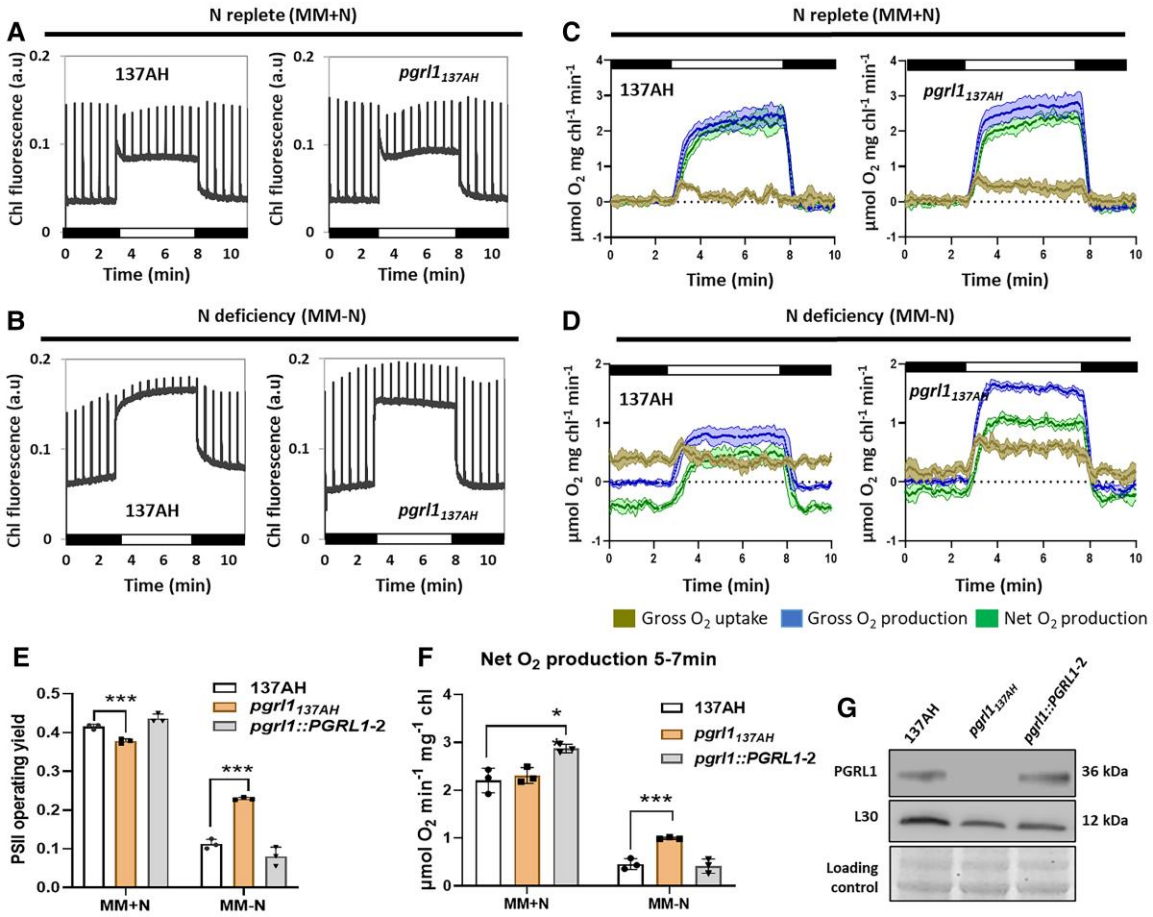

Figure 1. *Pgrl1* showed sustained photosynthesis after 2 d of N deficiency. **A,B)** Chlorophyll fluorescence was measured using a dual-PAM during the dark–light–dark transition from N-replete **A)** and N-deficient **B)** conditions. **C,D)** O_2 exchange rates were measured using a membrane inlet mass spectrometry (MIMS) during the dark–light–dark transition from N-replete **C)** and N-deficient **D)** conditions. Net O_2 evolution (green) was calculated as gross O_2 evolution (blue)—gross O_2 uptake (red). **E)** PSII (photosystem II) operating yield before and after 2 d of N deficiency measured using green actinic light (1,250 µmol photon m^{-2} s^{-1}, green LEDs) and calculated as ΦPSII = $(F_M'-Fs)/F_M'$ with F_M' the fluorescence value after saturating pulse, Fs the stationary fluorescence during actinic light exposure. **F)** The Net O_2 evolution before and after 2 d of N deficiency in the wild-type 137AH, $pgrl1_{137AH}$ and the complemented line *pgrl1*::*PGRL1*-2 calculated from panel C and D between 5 and 7 min. **G)** Immunoblot analysis of PGRL1 accumulation in the wild-type 137AH, *pgrl1* and the complemented line. L30 (50S ribosomal protein) antibody was used as a positive control. Coomassie blue staining was used as the loading control. Protein samples were obtained from 2 d N-starved cells. N-replete wild-type 137AH, $pgrl1_{137AH}$, and *pgrl1*::*PGRL1*-2 cells cultivated photoautotrophically with 1% CO_2 in air under continuous light (50 µmol photons m^{-2} s^{-1}) were transferred into N-free media for 2 d prior to measurements. All data represent means of 3 biologically independent samples (means ± SD). Asterisks represent statistically significant differences compared with the control 137AH (* $P < 0.05$, ** $P < 0.01$, and *** $P < 0.001$) using one-way ANOVA.

$P700^+$ in the environmental light, (2) PSI yield quantifies $P700^-$ during environmental acclimation that converts within the ms range to $P700^+$ upon a saturating light pulse, and (3) PSI acceptor side limitation represents a redox-inactive P700 pool (see Materials and Methods). In the absence of PGRL1/PGR5-controlled CEF the redox-inactive P700 pool is enhanced under CO_2-limiting conditions (Chaux et al. 2017b). This was also observed in the 137AH genetic background when $pgrl1_{137AH}$ was grown photoautotrophically under 1% CO_2 (Fig. 2, A and B). The failure to produce $P700^+$ in the light gradually developed within 0.5 s and persisted throughout the illumination period (Fig. 2, A and B). However, $pgrl1_{137AH}$ did not display lower PSI yields, typically detected in ambient CO_2 (DalCorso et al. 2008), since the diminished $P700^+$ was due to lower donor side limitation (Fig. 2B). The P700 differences in $pgrl1_{137AH}$ relied on PSII activity, pointing to a LEF/CEF entanglement. N deficiency further increased the $P700^+$ pool in a strictly donor side-dependent fashion in both wild-type and mutant. Nevertheless, $pgrl1_{137AH}$ displayed twice the PSI acceptor side limitation when PSII was active. Moreover, the mutant showed a delayed $P700^+$ formation within the first 200 ms of light when PSII was inhibited (Fig. 2A). The latter feature was also displayed in N-deficient CC125 under DCMU conditions (Supplementary Fig. S5A). This genetic background showed identical photo-oxidizable P700 pools between wild-type and mutant in the presence of N, with $pgrl1_{CC125}$-86 producing slightly higher acceptor side limitation (Supplementary Fig. S5B). N deficiency came at the expense of PSI yields and $pgrl1_{CC125}$-86 failed to alleviate the PSI acceptor side through sufficient donor side induction similar to $pgrl1_{137AH}$. These results suggest that PGRL1-controlled CEF facilitates the onset of photosynthetic control during photoautotrophic N deficiency by inducing a donor side limitation at PSI to alleviate its acceptor side redox pressure.

FLV-mediated O_2 photoreduction drives photosynthesis in *pgrl1* under N deficiency

Because light-dependent O_2 uptake can lead to the generation of extra ATP and support CO_2 fixation but at various levels depending on the mechanism involved (Peltier et al. 2024), we sought to test the nature of the light-dependent O_2 uptake mechanism activated in *pgrl1*

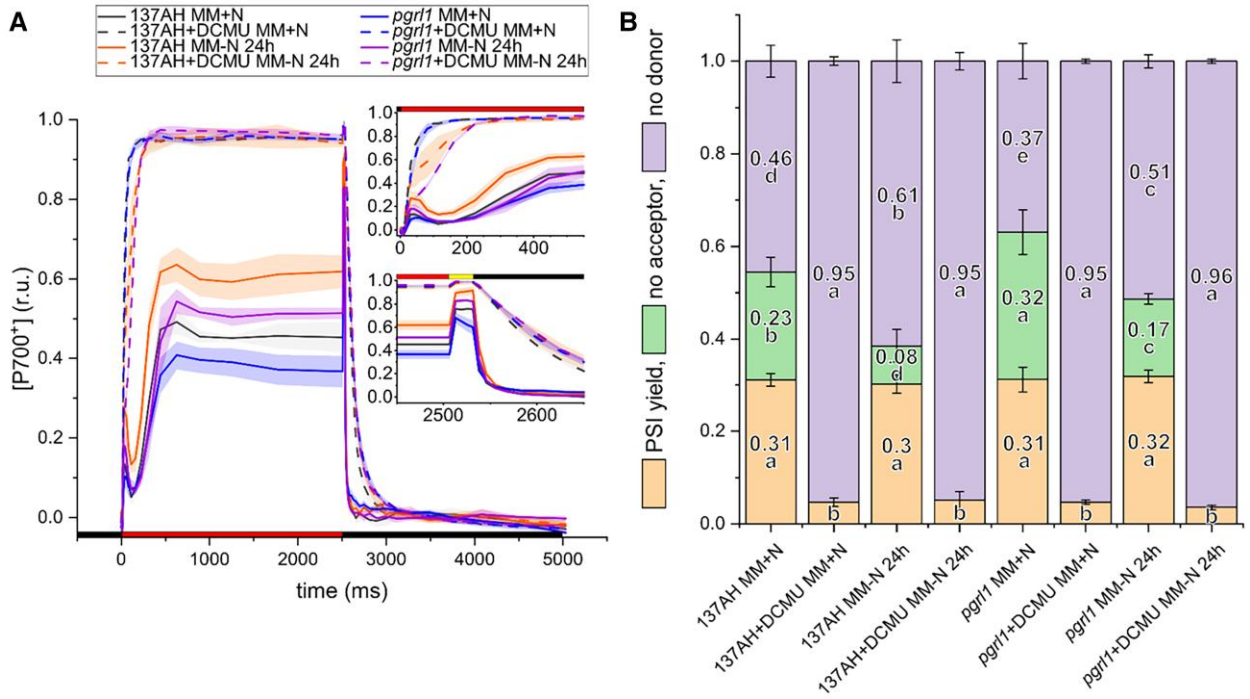

Figure 2. PSI oxidation is facilitated by PGRL1 under N deficiency. The influence of PGRL1 on the redox state of the primary photosystem I (PSI) donor, P700, was monitored in the genetic background 137AH **A,B**) and CC125 (Supplementary Fig. S5). Panel **A** shows raw kinetics (red/yellow/black bars: 490/3,000/0 μmol photons m^{-2} s^{-1}) in the presence and absence of photosystem II (PSII) inhibitor DCMU (means ± SD of 4 biologically independent samples). The insets represent enlarged displays of the beginning (top) and end (bottom) of the light period. Panel **B** quantifies the corresponding P700 pools at the end of the 2.5 s light period. Data represent means ± SD of 4 biological replicates and letters indicate parameter-specific significances using one-way ANOVA/Fisher-LSD, $P < 0.05$. At the time of quantification, P700 remained photo-oxidizable by a saturating pulse (PSI yield), was redox inactive (no acceptors) or was preoxidized (no donors). N-replete cells of wild-type 137AH and $pgrl1_{137AH}$ were cultivated photoautotrophically with 1% CO_2 in air under continuous light (50 μmol photons m^{-2} s^{-1}), and then transferred into N-free media for 24 h prior to measurements.

mutants during N deficiency (Fig. 1D). FLVs have been reported to be a major O_2 uptake mechanism in the light (Chaux et al. 2017a; Burlacot et al. 2018; Burlacot et al. 2022). *pgrl1 flvB* double mutants impaired in both PGRL1 and FLVB have been recently generated by crossing the $pgrl1_{137AH}$ with a FLVB deficient strain (*flvB21*) as described in Burlacot et al. (2022). Therefore, we used the parental lines as control strains (*flvB-21* and $pgrl1_{137AH}$) as well as sibling strains from the progeny of the crossing (WT1 and WT3) harboring both FLV and PGRL1 proteins (Supplementary Fig. S1A). The 2 mutants (*pgrl1 flvB-3* and *pgrl1 flvB-5*) and control sibling (WT1 and WT3) strains used throughout the manuscript have been chosen for having similar maximal photosynthesis under N-replete conditions (V_{Max}) (Burlacot et al. 2022; Peltier et al. 2024). For all the experiments, we kept the $pgrl1_{137AH}$ alongside with its control 137AH and *pgrl1::PGRL1-2*; *flvB* mutants (*flvB21*, *flvB208*, and *flvB308*) alongside with their control CC4533 and finally *pgrl1 flvB-3* and *pgrl1 flvB-5* alongside WT1 and WT3 as control. We evaluated steady-state O_2 exchange rate in $pgrl1_{137AH}$, *flvB* mutants as well as in the *pgrl1 flvB* double mutants after 2 d of N deficiency (Fig. 3). The light-dependent O_2 uptake was highly increased in $pgrl1_{137AH}$ but strongly impaired in *flvB* and *pgrl1 flvB* mutants (Fig. 3A; Supplementary Fig. S2) which mirrors what has been reported for N-replete conditions in the presence of atmospheric CO_2 level (Chaux et al. 2017a; Burlacot et al. 2022). Interestingly, while the gross O_2 uptake, the gross O_2 and the net O_2 evolution measured during steady-state photosynthesis remained high in $pgrl1_{137AH}$, no difference was detected between *flvB*, *pgrl1 flvB* mutants and their respective control lines (Fig. 3, B to D; Supplementary Fig. S2). Taken together, these data show that the absence of FLV-mediated O_2 photoreduction (in *pgrl1 flvB* mutants) suppresses the effect of N deficiency observed in $pgrl1_{137AH}$ strain. We conclude that FLV-mediated O_2 photoreduction, by maintaining PET reactions in *pgrl1*, allows net photosynthesis to be maintained at a high-level during N deficiency.

Cyt b_6f and PSI subunits were retained at higher levels in *pgrl1* under N deficiency

To gain insights into the mechanisms behind the high photosynthetic activity in *pgrl1* during N deficiency, we compared the relative abundance of representative catalytic core subunits from photosynthetic complexes in the $pgrl1_{137AH}$ and the 137AH wild-type during N deficiency (Fig. 4, A and D). Additionally, we also investigated potential changes in mitochondrial electron transport chain by probing Complex II (Cox IIB). We observed a sustained retention of the PSI subunit PsaD and Cyt *f* subunit of Cyt b_6f in $pgrl1_{137AH}$ compared with the 137AH (Fig. 4, A and D). Higher amounts of PsaD and Cyt *f* were observed in $pgrl1_{137AH}$ under N replete without any functional effect on PSII yield and Net O_2 evolution (Fig. 1, E and F; Fig. 4, A and D). As for the stimulated dark O_2 consumption (Fig. 1D), the amount of mitochondrial respiratory chains component Cox IIB was increased in the 137AH whereas it remains stable in the $pgrl1_{137AH}$ during N deficiency (Fig. 4A). It is worth noting that the hallmark of autophagy, i.e. ATG8 was barely detectable in the $pgrl1_{137AH}$ whereas it was highly induced in the 137AH under N deficiency (Fig. 4, A and D). All the other proteins tested accumulated to a similar amount in $pgrl1_{137AH}$ and 137AH (Fig. 4A). Note that higher amounts of Cyt *f* were also

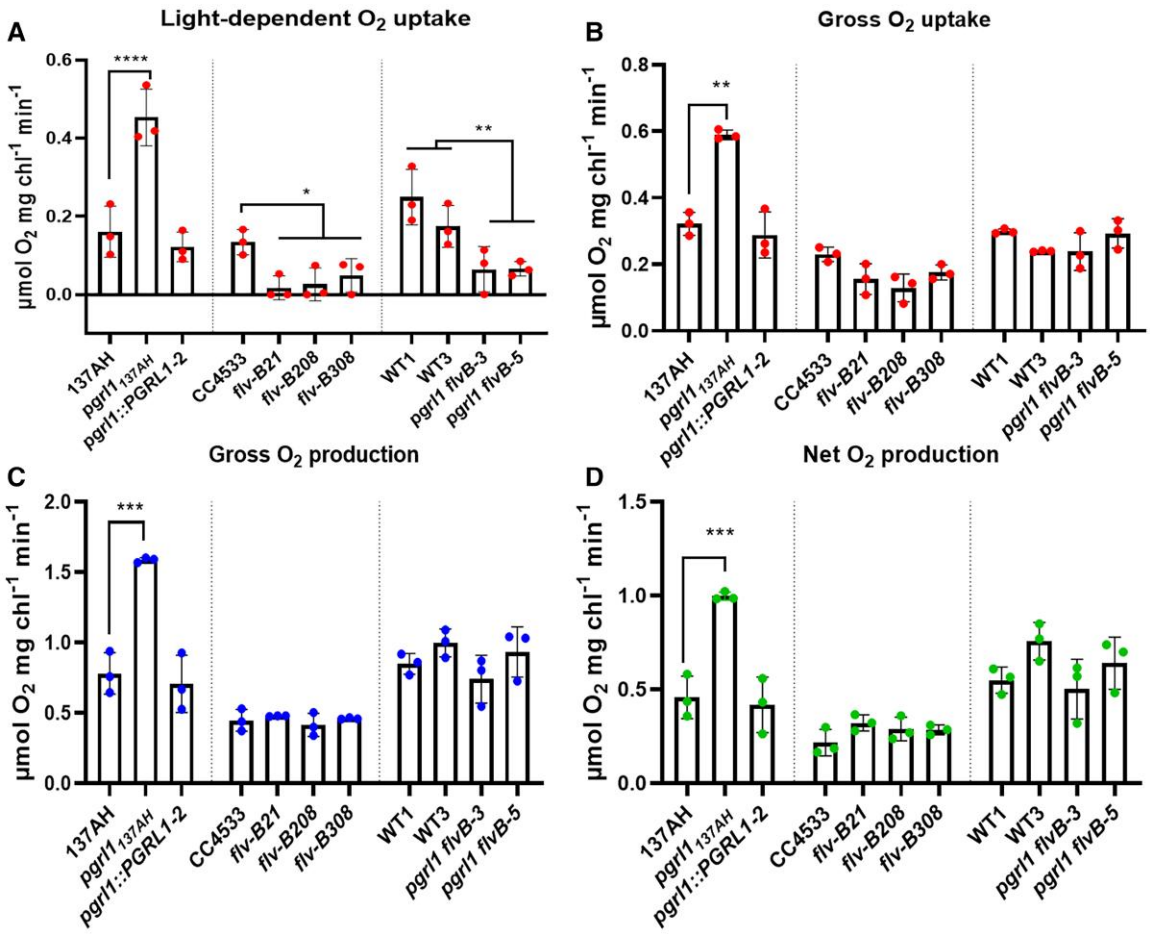

Figure 3. The photosynthesis in *pgrl1* is driven by FLV-mediated O_2 photoreduction under N deficiency. **A)** Light-dependent O_2 uptake attributed to FLV activity and calculated as the difference between the O_2 uptake during the 1st min of illumination and dark O_2 uptake as shown by Supplementary Fig. S2. **B)** Gross O_2 uptake measured between 5 and 7 min as shown by Supplementary Fig. S2. **C)** Gross O_2 evolution measured between 5 and 7 min as shown by Supplementary Fig. S2. **D)** Net O_2 evolution measured between 5 and 7 min as shown by Supplementary Fig. S2. O_2 exchange rates were measured using a MIMS in the presence of [^{18}O]-enriched O_2. Net O_2 evolution (green) was calculated as gross O_2 evolution (blue)—gross O_2 uptake (red). Cells cultivated photoautotrophically with 1% CO_2 in air under continuous light of 50 µmol photons m^{-2} s^{-1} were transferred into N-free media for 2 d prior to measurements or sampling for immunoblot. Data shown in A-D represent means of 3 biologically independent samples ± SD. Asterisks represent statistically significant difference compared with the wild-type strains (* $P < 0.05$, ** $P < 0.01$, *** $P < 0.001$, and **** $P < 0.0001$) using one-way ANOVA.

observed in a CRISPR-generated *pgrl1*$_{CC125}$ mutant when compared with CC125 in response to N deficiency (Supplementary Fig. S3I). We conclude from these experiments during N deficiency that the higher photosynthetic activity observed in mutants impaired in PGRL1 might result from a lower decrease in the amounts of PSI and Cyt b_6f complexes.

To test whether the retention of the PSI and Cyt b_6f observed in the *pgrl1*$_{137AH}$ are consequences of the existence of a FLV activity, similar immunoblot analyses were performed in the *flvB-21* and *pgrl1 flvB-3* mutants. Consistent to the photosynthetic activity, immunoblot analyses showed a similar accumulation of tested proteins in the *flvB-21* and *prgl1 flvB-3* compared with controls with the exception of lower PsaD and ATG8 in *prgl1 flvB-3* (Fig. 4, B and C and E and F). Representative original immunoblots showing the specificity of each antibody are reported as Supplementary Fig. S6.

Defects in CEF and PCEF altered carbon storage during N deficiency

Emerging literature suggests that alterations in energy management pathways affect biomass composition (Saroussi et al. 2017; Kong et al. 2018; Burlacot et al. 2019; Saroussi et al. 2019). Starch and TAGs are major forms of carbon storage in *Chlamydomonas* during N deficiency. Since the *pgrl1*$_{137AH}$ mutant shows a stronger net photosynthetic rate, we measured its ability to accumulate storage compounds. Starch accumulation was similar in *pgrl1*$_{137AH}$ and control lines under both N replete and deficiency (Fig. 5A; Supplementary Figs. S7B and S8A). In contrast, twice more TAG accumulation was observed in *pgrl1*$_{137AH}$ compared with the control lines under N deficiency whereas no difference was observed under N-replete condition (Fig. 5D; Supplementary Figs. S7A and S8D). Lipid droplet imaging confirmed the accumulation of higher TAG amounts (Supplementary Fig. S7C). However, *PGRL1* knockout mutants generated by Crispr–cas9 in the CC125 genetic background accumulated similar amount of TAGs, starch and chlorophyll in response to N deficiency compared with the CC125 control (Supplementary Fig. S9). Such a difference may be due to the fact that photosynthesis (assessed as PSII yield and net O_2 evolution) was lower in the *pgrl1*$_{CC125}$ background than in the *pgrl1*$_{137AH}$ background (Supplementary Fig. S3) thus limiting reserve accumulation; it may also indicate the existence of a metabolic limitation for storage compound accumulation in the CC125 background.

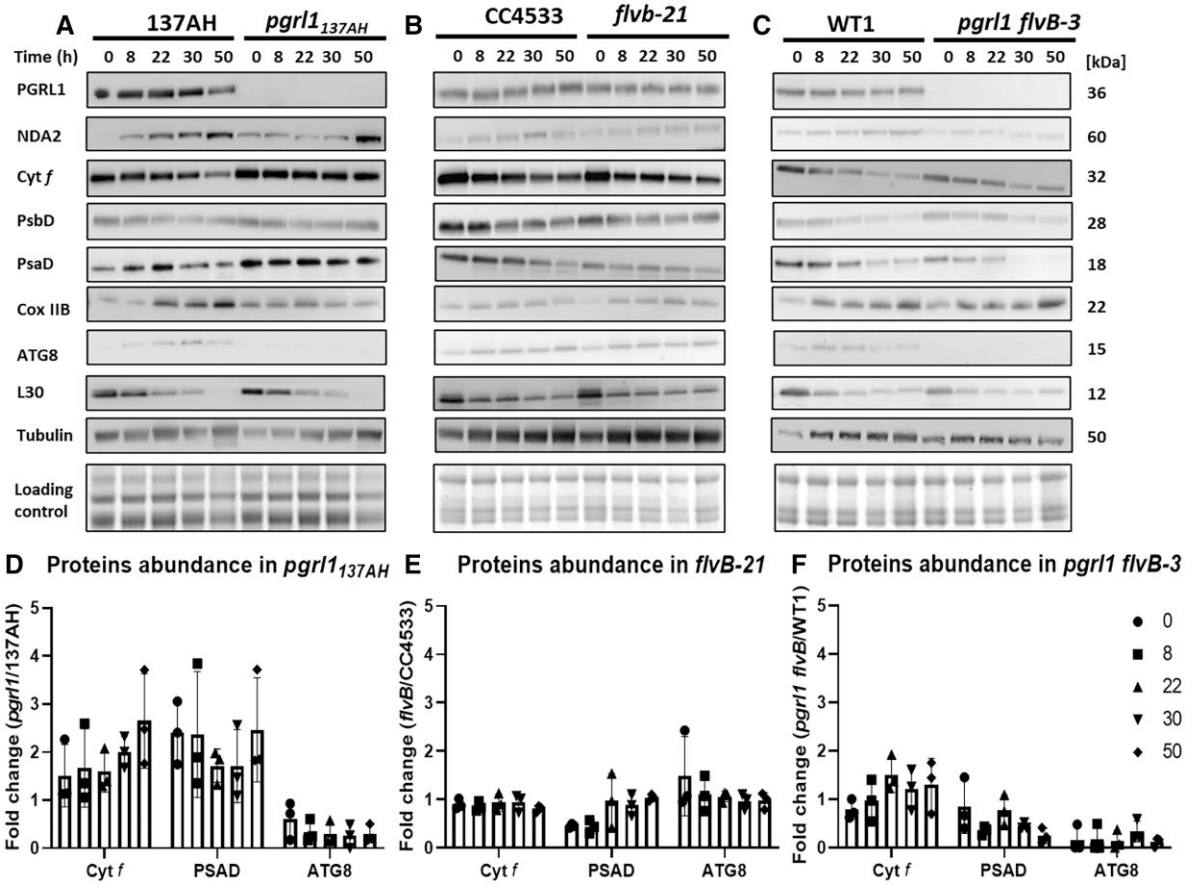

Figure 4. Cytochrome b_6f and PSI subunit PsaD were retained at higher levels in *pgrl1* under N deficiency. **A–C**) Immunodetection of photosynthetic proteins in the $pgrl1_{137AH}$, *flvB-21*, and *pgrl1 flvB-3* when compared with their controls during N deficiency. *pgrl1 flvB-3* is generated by crossing the $pgrl1_{137AH}$ with a FLVB deficient strain (*flvB21*) as described in (Burlacot et al. 2022). As a control, we used the sibling strain WT1 from the progeny of the crossing harboring both FLV and PGRL1 proteins. Cells were harvested at 0, 8, 22, 30, and 50 h of N deficiency. Samples were loaded at equal total protein amounts as shown by Coomassie blue staining. Shown are representative images of 3 biologically independent samples. The α-tubulin was used as housekeeping protein, whereas ATG8 and the chloroplast 50S ribosomal large subunit L30 are controls of N depletion (Upadhyaya et al. 2020; Crespo and Pérez-Pérez 2023). **D–F**) Histogrammes showing the abundance Cyt *f*, PsaD, and ATG8 proteins in the $pgrl1_{137AH}$, *flvB-21*, and *pgrl1 flvB-3* during N deficiency in the wild-type cells. The data shown represents the ratio of mutant over control strain. Data represent means of 3 biologically independent samples ± SD.

We then evaluated to what extent changes in photosynthesis affect biomass productivity by monitoring the dry weight, cell volume and cell number for 4 d before and during N deficiency. The $pgrl1_{137AH}$ and $pgrl1_{CC125}$ mutants produced similar biomass (assessed either by dry weight and cell volume) compared with their control 137AH and CC125 respectively (Supplementary Figs. S10 to S11). Note that $pgrl1_{137AH}$ cells form a multicellular structure under photoautotrophic conditions that prevent accurate cell counting (Supplementary Fig. S10). We conclude from these results that the higher photosynthetic activity in *pgrl1* mutants did not result in increased biomass productivity under N deficiency.

Under N replete, the *flvB* single mutants accumulated higher amounts of starch than the CC4533 wild-type but TAG accumulation was similar (Supplementary Fig. S8, B and E). Inversely, under N deficiency, the *flvB* accumulated lower amounts of TAG but starch accumulation was similar compared with CC4533 (Fig. 5, B and E). The double mutant $pgrl1_{137AH}$ *flvB* accumulated similar amounts of TAG and starch when compared with control strains either in N-replete or N-deprived conditions (Fig. 5, C and F; Supplementary Fig. S8, C and F).

We propose that both PGRL1 (CEF) and FLVs (PCEF), by having an antagonistic role during N deficiency, manage the redox landscape and carbon storage. It is worth pointing out that this modification of metabolism as a consequence of redox management depends not only on genetic background (137AH versus CC125) but also on the environmental state (+N versus −N) providing examples on the important role of gene–environment interaction in determining complex traits such as oil content.

Discussion

The ability of microalgae to coordinate their energy conversion (from light to chemical energy) to meet the metabolic demand is crucial for their survival in a constantly fluctuating environment. Mechanisms involved in photosynthesis regulations have been abundantly studied in response to light or CO_2 levels, but not much is known during nutrient deficiency when a massive reorientation of metabolic pathways occurs. In the absence of *N*, the major cellular energy sinks (cell division, protein biosynthesis, and photosynthetic CO_2 fixation) are restricted whereas the carbon and energy are stored as TAGs or starch. Moreover, the PET reactions are downregulated under N deficiency. However, we do not know whether the downregulation of PET is a mean to match cells energy status with the limited metabolic demand. In other words, how the metabolism accommodates when photosynthesis remains high during N deficiency is not well understood. In this

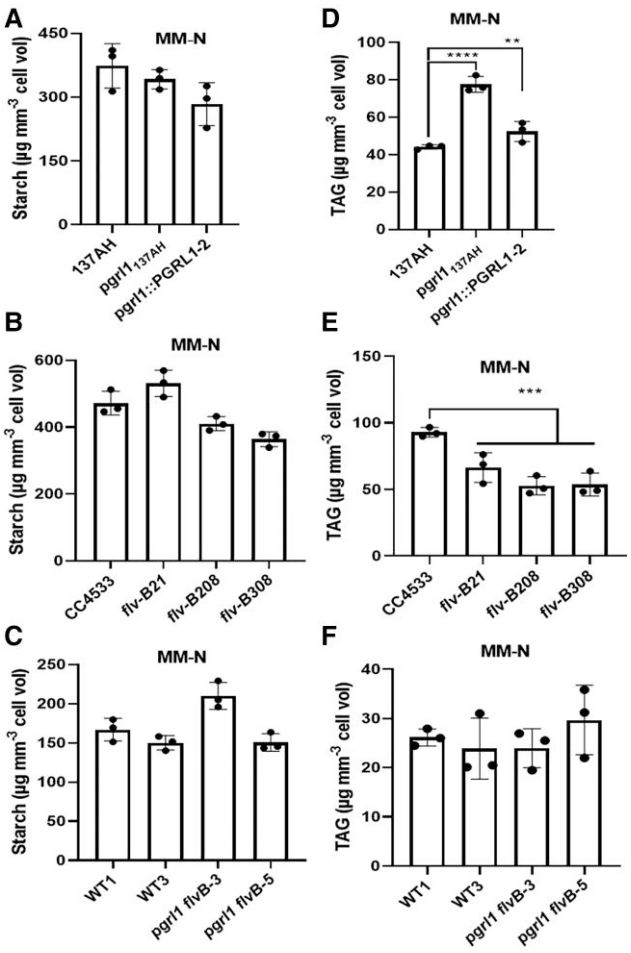

Figure 5. *Pgrl1* over accumulated TAGs under N deficiency. Starch **A–C**) and TAG **D–F**) quantification in N-deprived cells of $pgrl1_{137AH}$, *flvB*, and *pgrl1 flvB* mutants, respectively. Cells were cultivated photoautotrophically with 1% CO_2 in air under continuous light of 50 µmol photons m^{-2} s^{-1}. For N deficiency, cells were transferred into N-free media for 2 d prior to sampling for starch and TAG. All data shown represent means of 3 biologically independent samples (means ± SD). Asterisks represent statistically significant difference comparing mutants with their control strains (* $P < 0.05$, ** $P < 0.01$, and *** $P < 0.001$) using one-way ANOVA.

study, we demonstrated that PGRL1, which controls a CEF pathway, tunes PET during N deficiency. This tuning favors the photosynthetic control mechanism via Cyt b_6f to limit PSI donor availability (see below for details). Lack of PGRL1 resulted in sustained photosynthetic activity up to 2 d of N deficiency. The misregulation of the PGRL1/PGR5-controlled CEF is notorious for decreasing the photosynthetic control efficiency and rerouting of electrons into alternative acceptors such as H_2 production by hydrogenases or O_2 photoreduction by FLVs (Tolleter et al. 2011; Dang et al. 2014; Steinbeck et al. 2015). Here, we have further shown that the higher FLVs-mediated PCEF in *pgrl1* mutants channels excess electrons toward O_2 under N deficiency. PCEF thus counteracts PSI overreduction, likely facilitating ATP production and at the same time keeping PET active.

PGRL1/PGR5-controlled CEF contributes to photosynthetic control during N deficiency

The photosynthetic control refers to mechanisms that restrict the PET reactions mostly occurring in response to environmental fluctuations and is typically achieved on the level of the Cyt b_6f upon acidification of the thylakoid lumen. The PGRL1-PGR5-controlled CEF increases lumen acidification efficiency and has been shown to contribute to the photosynthetic control in land plants (Munekage et al. 2002; DalCorso et al. 2008; Yamamoto and Shikanai 2019) as well as in microalgae (Petroutsos et al. 2009; Tolleter et al. 2011; Johnson et al. 2014; Steinbeck et al. 2015; Buchert et al. 2020). The induction of the photosynthetic control results in PSI donor side limitation in the light which is typically determined in vivo via $P700^+$ optical readouts (Yamamoto and Shikanai 2019; Penzler et al. 2022; Zhou et al. 2023). Our results showed higher acceptor side limitation (at the expense of donor side limitation) in *pgrl1* mutants (Fig. 2; Supplementary Fig. S5) indicating that they are affected in the induction of the photosynthetic control. The decrease in Cyt b_6f abundance could be an additional cellular strategy to further restrict the PET toward PSI (higher donor side limitation in wild-type, Fig. 2; Supplementary Fig. S5). While the wild-type successfully relaxes the redox pressure on PSI and degrades Cyt b_6f under N deficiency, *pgrl1* mutants sustained PET and failed to degrade the Cyt b_6f. This dysfunctioning of the photosynthetic control in *pgrl1* (high acceptor side limitation and Cyt b_6f abundance; Figs. 2 and 4A), promotes the recruitment of stromal electron carriers such as FLVs and TAG biosynthesis (in 137AH background). Similar observations were reported under sulphur deprivation where deletion of PGRL1 or PGR5 resulted in sustained LEF toward H_2 production in *Chlamydomonas* (Tolleter et al. 2011; Steinbeck et al. 2015). Our work shows that impairing the accumulation of PGRL1 removes a bottleneck of photosynthetic electron flow during N deficiency under nonlimiting CO_2 conditions (Figs. 1 to 3; Supplementary Figs. S1 to S3). This characteristic of photosynthetic control makes PGRL1/PGR5-controlled CEF a promising target for improving photosynthetic yield under nutrients deficiency. Indeed, the control of photosynthesis under N deficiency has been seen as safety mechanisms protecting cells from phototoxicity (Munekage et al. 2002; Yamamoto and Shikanai 2019; Saroussi et al. 2023). Here, we show that thanks to the presence of FLVs, photosynthesis could be improved by removing PGRL1-controlled CEF during N deficiency under nonlimiting CO_2 conditions.

FLVs become predominant in the absence of PGRL1/PGR5-controlled CEF

So far, a compensation mechanism between PGRL1 and FLVs has been reported during algal adaptation to light or low-CO_2 conditions (Dang et al. 2014; Burlacot et al. 2022; Peltier et al. 2024). Under high light or low-CO_2 conditions, the increased activity of FLVs in the PGRL1-deficient strain does not improve the net photosynthesis despite its strong efficiency in generating ATP (Burlacot et al. 2022; Peltier et al. 2024). Similar compensation has also been observed in land plants where orthologous expression of FLVs rescues the *pgr5* mutants phenotype without further improving photosynthesis (Wada et al. 2018; Yamamoto and Shikanai 2019) although some levels of increased biomass were measured in wild-type Arabidopsis expressing FLVs under light fluctuations thanks to the protective role of FLVs in these conditions (Basso et al. 2022). In contrast, our results suggest that under N deficiency, FLVs and PGRL1 have an antagonistic role. Indeed, the increased light-dependent O_2 uptake in the PGRL1-deficient strains, mostly attributed to the activity of FLVs (see Fig. 3A), was accompanied by a higher net photosynthesis (Fig. 3D; Supplementary Fig. S2). This indicates that rather than compensating each other,

PGRL1 indirectly controls the activity of FLVs by limiting the maximal electron flow capacity. We therefore propose that Cyt b6f preservation observed in *pgrl1* under N deficiency, but not in *pgrl1 flvB* double mutants (Fig. 4, A and D), may result from the activity of FLVs-mediated PCEF draining electrons from the photosynthetic chain and indirectly preventing Cyt b6f from degradation.

Because CEF and PCEF are dominant pathways for supplying extra ATP in addition to LEF in the chloroplast, we were expecting that the removal of both PGRL1 and FLVs would have more severe consequences on cell physiology and metabolism as it was observed when CO_2 is limiting (Burlacot et al. 2022). Instead, we observed similar photosynthetic activity and TAG biosynthesis in the *pgrl1 flvB* double mutants as their control strains (Figs. 3 and 5), i.e. the additional removal of FLVs suppressed the phenotype of PGRL1 deficiency. A third pathway generating the energy required for photosynthetic CO_2 fixation and ensuring redox dissipation could be operating in the double mutant *pgrl1 flvB*. Both the NDA2-dependent CEF (Desplats et al. 2009; Saroussi et al. 2016) or a chloroplast-mitochondria electron flow (CMEF) (Peltier et al. 2024) could be good candidates. NDA2 protein level was shown to increase during air photoautotrophic N deficiency under atmospheric CO_2 level and the CEF rate in *Chlamydomonas* was decreased by 50% in *nda2* mutants (Saroussi et al. 2016). However, we observed a similar protein level of NDA2 in the *pgrl1 flvB* as their control lines (Fig. 4C). Nevertheless, the protein level might not always correspond to the activity and other regulatory mechanisms (e.g. phosphorylation or redox regulation) can modulate enzyme activity. Additionally, the stimulated mitochondrial respiration rates as well as increased in Cox IIB protein level during N-deficiency in all the strains (except $pgrl1_{137AH}$) (Fig. 4; Supplementary Fig. S3) points to a strong activity of CMEF (Burlacot et al. 2022; Peltier et al. 2024), which might compensate for CEF and PCEF deficiency in *pgrl1 flvB* N-deprived cells. CMEF may have 2 distinct roles, either to supply additional ATP (Peltier et al. 2024) or favor dissipation of excess NAD(P)H that likely accumulate in *pgrl1 flvB* mutants (Cardol et al. 2003; Dang et al. 2014; Kaye et al. 2019). In the context of generating extra ATP, the Cox IIB pathways could take over the AOX1 alternative oxidase pathway because of its efficiency in generating ATP (Peltier et al. 2024). Further investigation would be required to identify the mechanisms generating ATP in the absence of PGRL1 and FLVs. Altogether, we conclude that FLVs maintain high photosynthetic activity under N deficiency in the absence of PGRL1 by channeling excess electrons toward O_2 meanwhile generating ATP for CO_2 and downstream metabolic pathways (TAG production).

Relationship between cellular redox landscape and carbon storage

A major biotechnological challenge in algal domestication for biofuel is the tradeoff between growth and lipid productivity. In *Chlamydomonas* as in many other microalgae, starch and TAG massively accumulate but mostly under stress conditions in particular N deficiency when cell division stops and productivity is impaired. Considerable efforts have focused on the study of the molecular mechanisms behind the onset of reserve accumulation by monitoring omics responses to a stress (Miller et al. 2010; Blaby et al. 2013; Schmollinger et al. 2014; Zienkiewicz et al. 2016; Takeuchi and Benning 2019), or focused on specific steps of fatty acid and TAG biosynthesis, which have resulted in some limited improvement in productivity (Kong et al. 2019; Li-Beisson et al. 2019). Improving productivity requires a better understanding of the crosstalk between photosynthetic carbon fixation, environmental signals and the redox balance, which all govern reserve accumulation (Geigenberger et al. 2005; Michelet et al. 2013; Geigenberger and Fernie 2014). Here by studying mutants affected in CEF and PCEF, we explored the relationships between the cellular redox status and carbon storage.

The increased accumulation of TAG but not starch observed in the PGRL1-deficient strain (137AH background) under N deficiency (Fig. 5, A and D) is a consequence of continuous production of NADPH and ATP through PCEF-dependent PET. In line with our finding, the *Chlamydomonas pgd1* mutants (e.g. *Plastid galactoglycerolipid degradation 1)* with reduced LEF rate (less ATP and NADPH) are shown to produce less TAG under N starvation (Li et al. 2012; Du et al. 2018). The report that the *pgrl1* mutant made less TAG than wild-type under mixotrophic conditions (Chen et al. 2015) is not surprising. It is well known that the bioenergetics of *Chlamydomonas* under photoautotrophic conditions differ from mixotrophic conditions (Johnson and Alric 2012; Johnson and Alric 2013; Saint-Sorny et al. 2022). The presence of acetate can drastically affect cellular bioenergetics levels, i.e. its uptake consumes ATP and its metabolism produces NADH, therefore further favoring oil synthesis (Goodson et al. 2011; Johnson and Alric 2012; Johnson and Alric 2013; Goodenough et al. 2014). TAGs accumulation was different in the CC125 background where the $pgrl1_{CC125}$ mutant made similar amounts of TAGs as its background strain (Supplementary Fig. S9, A and B). This seems not surprising when we consider that TAG accumulation is a metabolic consequence of changes in chloroplast redox state and in photosynthetic performance. The preservation of PSII yield and net O_2 evolution was less dramatic in the CC125 background than in the 137AH background, which could be one of the reasons behind strain-dependent phenotype. Taken together, these findings further point to the fact that oil content is a complex trait, and it is the consequence of the interaction between genetic makeup, its metabolic flexibility and the capacity of the extent of a given cell's response to environmental changes.

In contrast to $pgrl1_{137AH}$, the *flvB* mutants accumulated lower amounts of TAGs under N deficiency, and no difference in TAG was observed in the *pgrl1 flvB* double mutants, consisting again with the profile in photosynthetic performance and with their antagonistic roles. The *flvB* mutants accumulated a higher amount of starch under N sufficient condition though. To conclude, this work further points to the importance of the role redox management on carbon allocation and storage, and that this effect is dependent on many factors including the genetic background, the trophic style, as well as the nutrient status.

Materials and methods

Growth conditions and strains

The $pgrl1_{137AH}$ (from the background 137AH which is an isolate of 137c mt- nit1 nit2) with its complementing strain (*pgrl1::PGRL1-2*), *flvB* mutants (*B-21*, *B-208*, and *B-308*) from the background CC-4533 and the *pgrl1 flvB* double mutants with their respective controls WT1 and WT3 obtained by crossing $pgrl1_{137AH}$ with *flvB-21* were previously described (Tolleter et al. 2011; Chaux et al. 2017a; Burlacot et al. 2022). $pgrl1_{CC125}$ mutants were generated in the CC125 background using CRISPR–Cas9 (see below). All the information about the strains used is reported in Supplementary Table S1. Cells were routinely cultivated in an incubation shaker (INFORS Multitron pro) maintained at 25 °C, with

120 rpm shaking and constant illumination at 50 µmol m^{-2} s^{-1}. Fluorescent tubes delivering white light enriched in red wavelength supplied lightings in the INFORS. All experiments were performed under photoautotrophic conditions with the HS minimum medium with or without nitrogen source (MM and MM-N) buffered with 20 mM MOPS at pH 7.2 in air enriched with 1% CO_2. Due to cell aggregation in the 137AH background (notably the *pgrl1* mutant) that prevent accurate cell counting, total cellular volume was measured using a Multisizer 4 Coulter counter (Beckman Coulter) and the different strains were diluted to reach a similar cellular concentration before N deficiency experiments. For dry weight, cells were dried on Whatman filter discs overnight in a 100 °C oven. To induce N deficiency, 25 mL of cells grown under N-replete condition (at ~ 3 million cells/mL) were centrifuged at 2,000*g* for 3 min washed twice with MM-N medium and resuspended in fresh MM-N.

Generation of *pgrl1* mutant in the CC125 background

Chlamydomonas mutants harboring targeted insertion in the *PGRL1* locus was generated in the CC-125 background (mt+, nit–) using CRISPR/Cas-9 mutagenesis. *Chlamydomonas* strain CC-125 (*nit1*; *nit2*; *mt+*) was grown in tris-acetate-phosphate (TAP) media under continuous illumination of 50 µmol photons m^{-2} s^{-1} at 22 °C. Single guide RNAs (sgRNAs) (Supplementary Table S2) were designed by CHOPCHOP (Labun et al. 2019) using version 5.6 of the *C. reinhardtii* genome. Ribonucleic proteins (RNPs) were prepared by duplexing the sgRNA (23% volume per volume—v/v-) and Cas-9 (IDT, Ref# 427093062.) (19% v/v) with duplex buffer (IDT, Ref# 325470395) (60% v/v). After treatment with autolysin for 3 h without shaking, cells were washed with TAP growth media supplemented with 40 mM of sucrose, resuspended with the same supplemented media to 2×10^8 cells mL^{-1}, and electroporated in the presence of hygromycin resistance cassette (2 µg mL^{-1}) and RNP mixture. After 10 min at room temperature, cells were resuspended in 10 mL of TAP growth media supplemented with 40 mM of sucrose and left without shaking overnight in dim light (10 to 20 µmol photons m^{-2} s^{-1}). Hygromycin resistant transformants were selected on TAP-agar plates containing hygromycin (20 µg mL^{-1}). sgRNA targeted regions were amplified via polymerase chain reaction (PCR) to check for full or partial insertion of the hygromycin resistance cassette at the target site (Supplementary Table S3 and Fig. S4).

Measurement of chlorophyll fluorescence using a PAM

Chlorophyll fluorescence was measured using a PAM fluorimeter (Dual-PAM 100, Walz GmbH, Effeltrich, Germany) on the membrane inlet mass spectrometry (MIMS) chamber as described in (Burlacot et al. 2018) using green actinic light (1,250 µmol photon m^{-2} s^{-1}, green LEDs). Cells were dark-adapted for 10 min and aerated by stirring in MIMS chamber. Red saturating flashes (8,000 µmol photons m^{-2} s^{-1}, 600 ms) were delivered to measure the maximum fluorescence (FM) every 30 s (before and upon actinic light exposure). The *Fv/Fm* parameter was calculated as $Fv/Fm = (Fm-Fo)/Fm$ where F_0 is the basal fluorescence obtained with the measuring light and Fm the fluorescence emitted after saturating pulse (Maxwell and Johnson 2000). PSII operating yield (ΦPSII) was calculated as $\Phi PSII = (F_M'-Fs)/F_M'$ with F_M' the fluorescence value after saturating pulse, *Fs* the stationary fluorescence during actinic light exposure.

O_2 exchange measurement using MIMS

O_2 exchanges were measured in the presence of [^{18}O]-enriched O_2 using a water-jacketed, thermoregulated (25 °C) reaction vessel coupled to a mass spectrometer (model Prima ΔB; Thermo Electronics) through a membrane inlet system (Burlacot et al. 2020). The cell suspension (1.5 mL) was placed in the reaction vessel and bicarbonate (10 mM final concentration) was added to reach a saturating CO_2 concentration. One hundred microliters of [^{18}O]-enriched O_2 (99% $^{18}O_2$ isotope content; Euriso-Top) was bubbled at the top of the suspension just before vessel closure and gas exchange measurements. O_2 exchanges were measured during a 3 min period in the dark, then the suspension was illuminated at 1,250 µmol photons m^{-2} s^{-1} for 5 min using green LEDs followed by 3 min in the dark. Isotopic O_2 species [$^{18}O^{18}O$] (m/e = 36), [$^{18}O^{16}O$] (m/e = 34), and [$^{16}O^{16}O$] (m/e = 32) were monitored, and O_2 exchange rates were determined (Burlacot et al. 2020). Argon gas was used to correct O_2 exchange measured by the spectrometer as described in Burlacot et al. (2020).

Redox state measurements of the PSI primary electron donor P700

The Redox state of PSI primary electron donor P700, were obtained from optical signals (705 to 740 nm) using a Joliot-type spectrophotometer (JTS-150, Spectrologix USA), described in detail elsewhere (Klughammer and Schreiber 1994; Buchert et al. 2020; Buchert et al. 2022). Harvested cells (2 min, 4,000 rpm, 22 °C) were resuspended in cuvettes to comparable densities in growth medium containing 20% Ficol (*w/v*). Samples were subjected to 2.5 s alterations of dark/light (490 µmol photon m^{-2} s^{-1}, 630 nm LEDs), leading to a partial P700 preoxidation during the light period (donor side limitation). Additional fractions of photo-oxidizable P700 (PSI yield) were obtained by a 25 ms saturating pulse before the dark period, revealing nonoxidizable P700 (acceptor side limitation) after comparison to fully oxidized P700 when measured in the presence of 20 µM 3-(3,4-dichlorophenyl)-1,1-dimethylurea (DCMU).

Starch quantification

Starch was quantified from 1 mL of culture containing ~3 to 6 million cells. Briefly, cells were harvested by centrifugation at 13,000 *g* for 4 min at 4 °C. Pellet was resuspended into 1 mL of methanol, mixed vigorously, and stored at –20 °C before analysis. The supernatants were removed and the residual methanol was evaporated from the pellets incubated at room temperature in a fume hood. Pellets were resuspended in 400 µL of distilled water and autoclaved for 20 min at 120 °C to solubilize the starch polymer. Total starch was quantified using an enzymatic starch assay kit (Sigma-Aldrich; ref. SA-20) following the manufacturer's instructions. Glucose converted from the starch was quantified using an automated YSI 2,700 glucose analyzer (YSI Life Sciences) previously calibrated using a commercial glucose standard.

TAG quantification

Exponentially grown cells (~20 millions) were harvested by centrifugation at 4,000 *g* for 3 min at 4 °C. Pellets were resuspended in 1 mL of hot isopropanol containing 0.01% butylated hydroxytoluene (BHT) (w/v) for 10 min at 85 °C to quench lipases (Légeret et al. 2016). A mixture of methyl tert-butyl ether (MTBE):H_2O (3/1, v/v) was added to extract lipids, vortexed and allow for phase separation. Finally, lipids were recovered from the upper organic phase after centrifugation at 4,000 *g* for 3 min at 4 °C. Solvent was evaporated under a stream of N_2 and total lipid extract was dissolved in 200 µL of chloroform:methanol (2:1 v/v) prior to

analysis. TAG was separated from other lipid classes by thin layer chromatography (TLC) and quantified based on densitometry method via comparing a standard curve generated from loading known amount of the standard TAG51:0 (17:0/17:0/17:0) (Sigma-Aldrich) to the same plate as described previously in Siaut et al. (2011). Total fatty acids were quantified as described in (Siaut et al. 2011). Briefly, the extracted lipids were converted to FAMEs by acid-catalyzed transmethylation, extracted into hexane and analyzed by gas chromatography coupled to flame ionization detector and mass spectrometry (GC-FID-MS) (Agilent 7890A GC and Agilent 5975C MS, Agilent Technologies, Palo Alto, CA, USA).

Immunoblot

For protein extraction, exponentially grown cells (3 mL at around 10 µg mL^{-1} of chlorophyll) were harvested by centrifugation at 4,000 *g* for 3 min at 4 °C. Pellets were resuspended in 200 µL of 1% SDS, to which 800 µL of cold acetone were added to extract chlorophyll and the suspension was incubated for 30 min at −20 °C. Samples were then centrifuged for 10 min, 13,000 *g* at 4 °C to precipitate proteins. Chlorophyll concentration was measured by spectrophotometry from supernatant. The protein pellet was resuspended with Novex Nupage LDS buffer 1× (Invitrogen) containing reducing agent DTT, at a final volume corresponding to 1 µL per 0.1 µg chlorophyll measured (corresponding to 1 µg $µL^{-1}$ of protein), the resuspended proteins were then denatured for 20 min at 70 °C. Ten micrograms of protein were loaded on Novex Nupage Bis tris 12% (Invitrogen) gel, migrated 1 h at 190 V in Novex Nupage MOPS (Invitrogen) buffer (or Novex Nupage MES (Invitrogen) according to protein molecular weight and transferred to nitrocellulose membrane using semidry transfer technique. Immunodetection was performed using antibodies raised against PGRL1 (Tolleter et al. 2011), NDA2 (Desplats et al. 2009). Other antibodies were ordered from Agriserea for PSBD (AS06 146) 1/10000, PSAD (AS09 461), Cyt *f* (AS06 119) 1/500, Cox IIB (AS06 151) 1/5000, ATG8 (AS14 2769) 1/2,000 (Upadhyaya et al. 2020; Crespo and Pérez-Pérez 2023), 50S ribosomal protein L30 (AS08 331) 1/1,000 and α-Tubulin (AS10 680) 1/1000. Secondary antirabbit peroxidase-conjugated antibodies (Sigma-Aldrich; no. AQ132P) (1/10,000) were used for the detection with the G:BOX Chemi XRQ system (Syngene) using ECL detection reagents (GE Healthcare). Images were captured with a CCD camera equipped with a GeneSys Image Acquisition Software (Syngene).

Statistical analysis

One-way ANOVA using GraphPad Prism (GraphPad Software) was used to perform statistical analysis. The *P*-values were computed by one-way ANOVA test with uncorrected *P*-values. Shown are grouping of strains into statistical families according to *P*-values indicated by asterisk (* for $P \leq 0.05$; ** for $P \leq 0.01$; *** for $P \leq 0.001$, and **** for $P \leq 0.0001$) or letters indicating parameter-specific significances. The statistical significance (α) was set as 0.05 (5%).

Accession numbers

Sequence data from this article can be found in the GenBank/EMBL data libraries under accession numbers Cre07.g340200 (PGRL1) and Cre16.g691800 (FLVB).

Acknowledgments

We thank Bertrand Legeret for maintaining the HelioBiotec lipidomics platform and Mallaury Cabanel for assistance in performing some of the immunoblots. We thank Hannah Menghis for her help in generating Crispr–cas9 mutants. We also acknowledge the ZoOM microscopy facility.

Author contributions

Y.L.-B., G.P., A.B., and O.D. conceived the study. Y.L.-B., G.P., and A.B. provided supervision. O.D. performed most of the experiments. P.A., M.B., and O.D. carried out biochemical experiments. M.B. and O.D. performed starch and lipid analysis. G.P. supervised the MIMS experiments. C.S., S.K.M., and J.I. generated the CRISPR-mediated mutant lines under the supervision of A.B., F.B., and M.H. performed and analyzed the P700 measurements. O.D. drafted the manuscript with contributions from A.B., G.P, F.B., M.H., and Y.L.-B.

Supplementary data

The following materials are available in the online version of this article.

Supplementary Figure S1. PSII activity measurement using PAM in *pgrl1*$_{137AH}$, *flvB* and *pgrl1 flvB* mutants upon N deficiency.

Supplementary Figure S2. O_2 exchange measurement under N replete and deficiency in *pgrl1*$_{137AH}$, *flvB* and *pgrl1 flvB* mutants.

Supplementary Figure S3. Photosynthetic activity in CRISPR–Cas9 generated *pgrl1*$_{CC125}$ mutants.

Supplementary Figure S4. Isolation of the 3 independent CRISPR mutants of *pgrl1* in CC125 background.

Supplementary Figure S5. Redox state measurements of P700 in *pgrl1*$_{CC125}$-86 mutant.

Supplementary Figure S6. Representative uncropped immunoblots from Fig. 4.

Supplementary Figure S7. Evaluation of carbon storage during N deficiency in *pgrl1*$_{137AH.}$

Supplementary Figure S8. Starch and TAG production in *pgrl1*$_{137AH}$, *flvB* and *pgrl1 flvB* mutants.

Supplementary Figure S9. Starch, TAG and chlorophyll content in *pgrl1*$_{CC125}$ mutants.

Supplementary Figure S10. Evaluation of biomass production during N deficiency in *pgrl1*$_{137AH}$.

Supplementary Figure S11. Evaluation of biomass production during N deficiency in *pgrl1*$_{cc125}$.

Funding

O.D. thanks The French Atomic Energy and Alternative Energy Commission (CEA) for a PhD scholarship. G.P. and Y.L.-B. acknowledge the continuous financial support of CEA (LD-power, CO2Storage). A.B. acknowledges the support of the Carnegie Institution for Science. M.H. (DFG Research Unit FOR 5573) and F.B. (BU 3426/3-1) acknowledge Deutsche Forschungsgemeinschaft for funding.

Conflict of interest statement: There are no conflicts of interest.

Data availability

All data are incorporated into the article and its online supplementary material.

References

Allen JF. Photosynthesis of ATP—electrons, proton pumps, rotors, and poise. *Cell*. 2002:110(3):273–276. https://doi.org/10.1016/S0092-8674(02)00870-X

Allen JF. Cyclic, pseudocyclic and noncyclic photophosphorylation: new links in the chain. *Trends Plant Sci*. 2003:8(1):15–19. https://doi.org/10.1016/S1360-1385(02)00006-7

Bailleul B, Berne N, Murik O, Petroutsos D, Prihoda J, Tanaka A, Villanova V, Bligny R, Flori S, Falconet D, *et al*. Energetic coupling between plastids and mitochondria drives CO_2 assimilation in diatoms. *Nature*. 2015:524(7565):366–369. https://doi.org/10.1038/nature14599

Basso L, Sakoda K, Kobayashi R, Yamori W, Shikanai T. Flavodiiron proteins enhance the rate of CO2 assimilation in Arabidopsis under fluctuating light intensity. *Plant Physiol*. 2022:189(1):375–387. https://doi.org/10.1093/plphys/kiac064

Blaby IK, Glaesener AG, Mettler T, Fitz-Gibbon ST, Gallaher SD, Liu B, Boyle NR, Kropat J, Stitt M, Johnson S, *et al*. Systems-level analysis of nitrogen starvation-induced modifications of carbon metabolism in a *Chlamydomonas reinhardtii* starchless mutant. *Plant Cell*. 2013:25(11):4305–4323. https://doi.org/10.1105/tpc.113.117580

Bonente G, Ballottari M, Truong TB, Morosinotto T, Ahn TK, FlemingGR, Niyogi KK, Bassi R. Analysis of LhcSR3, a protein essential for feedback De-excitation in the green alga *Chlamydomonas reinhardtii*. *PLoS Biol*. 2011:9(1):e1000577. https://doi.org/10.1371/journal.pbio.1000577

Buchert F, Mosebach L, Gäbelein P, Hippler M. PGR5 is required for efficient Q cycle in the cytochrome b6f complex during cyclic electron flow. *Biochem J*. 2020:477(9):1631–1650. https://doi.org/10.1042/BCJ20190914

Buchert F, Scholz M, Hippler M. Electron transfer via cytochrome b 6 f complex displays sensitivity to antimycin A upon STT7 kinase activation. *Biochem J*. 2022:479(1):111–127. https://doi.org/10.1042/BCJ20210802

Burlacot A, Burlacot F, Li-Beisson Y, Peltier G. Membrane inlet mass spectrometry: a powerful tool for algal research. *Front Plant Sci*. 2020:11:1302. https://doi.org/10.3389/fpls.2020.01302

Burlacot A, Dao O, Auroy P, Cuiné S, Li-Beisson Y, Peltier G. Alternative photosynthesis pathways drive the algal CO_2-concentrating mechanism. *Nature*. 2022:605(7909):366–371. https://doi.org/10.1038/s41586-022-04662-9

Burlacot A, Peltier G, Li-Beisson Y. Subcellular energetics and carbon storage in *Chlamydomonas*. *Cells*. 2019:8(10):1154. https://doi.org/10.3390/cells8101154

Burlacot A, Sawyer A, Cuiné S, Auroy-Tarrago P, Blangy S, Happe T, Peltier G. Flavodiiron-mediated O2 photoreduction links H2 production with CO2 fixation during the anaerobic induction of photosynthesis. *Plant Physiol*. 2018:177(4):1639–1649. https://doi.org/10.1104/pp.18.00721

Cardol P, Gloire G, Havaux M, Remacle C, Matagne R, Franck F. Photosynthesis and state transitions in mitochondrial mutants of *Chlamydomonas reinhardtii* affected in respiration. *Plant Physiol*. 2003:133(4):2010–2020. https://doi.org/10.1104/pp.103.028076

Chaux F, Burlacot A, Mekhalfi M, Auroy P, Blangy S, Richaud P, Peltier G. Flavodiiron proteins promote fast and transient O2 photoreduction in Chlamydomonas. *Plant Physiol*. 2017a:174(3):1825–1836. https://doi.org/10.1104/pp.17.00421

Chaux F, Johnson X, Auroy P, Beyly-Adriano A, Te I, Cuiné S, Peltier G. PGRL1 and LHCSR3 compensate for each other in controlling photosynthesis and avoiding photosystem I photoinhibition during high light acclimation of Chlamydomonas cells. *Mol Plant*. 2017b:10(1):216–218. https://doi.org/10.1016/j.molp.2016.09.005

Chen H, Hu J, Qiao Y, Chen W, Rong J, Zhang Y, He C, Wang Q. Ca2+-regulated cyclic electron flow supplies ATP for nitrogen starvation-induced lipid biosynthesis in green alga. *Sci Rep*. 2015:5(1):15117. https://doi.org/10.1038/srep15117

Crespo JL, Pérez-Pérez ME. Monitoring autophagic flux in the model single-celled microalga *Chlamydomonas reinhardtii*. In: Lois LM, Trujillo M, editors. *Plant proteostasis: methods and protocols*. New York, NY: Springer US; 2023. p. 123–134.

DalCorso G, Pesaresi P, Masiero S, Aseeva E, Schünemann D, Finazzi G, Joliot P, Barbato R, Leister D. A complex containing PGRL1 and PGR5 is involved in the switch between linear and cyclic electron flow in Arabidopsis. *Cell*. 2008:132(2):273–285. https://doi.org/10.1016/j.cell.2007.12.028

Dang K-V, Plet J, Tolleter D, Jokel M, Cuiné S, Carrier P, Auroy P, Richaud P, Johnson X, Alric J, *et al*. Combined increases in mitochondrial cooperation and oxygen photoreduction compensate for deficiency in cyclic electron flow in *Chlamydomonas reinhardtii*. *Plant Cell*. 2014:26(7):3036–3050. https://doi.org/10.1105/tpc.114.126375

Desplats C, Mus F, Cuiné S, Billon E, Cournac L, Peltier G. Characterization of nda2, a plastoquinone-reducing type II NAD(P)H dehydrogenase in Chlamydomonas chloroplasts. *J Biol Chem*. 2009:284(7):4148–4157. https://doi.org/10.1074/jbc.M804546200

Du E, Terrer C, Pellegrini AFA, Ahlström A, van Lissa CJ, Zhao X, Xia N, Wu X, Jackson RB. Global patterns of terrestrial nitrogen and phosphorus limitation. *Nat Geosci*. 2020:13(3):221–226. https://doi.org/10.1038/s41561-019-0530-4

Du Z-Y, Lucker BF, Zienkiewicz K, Miller TE, Zienkiewicz A, Sears BB, Kramer DM, Benning C. Galactoglycerolipid lipase PGD1 is involved in thylakoid membrane remodeling in response to adverse environmental conditions in Chlamydomonas. *Plant Cell*. 2018:30(2):447–465. https://doi.org/10.1105/tpc.17.00446

Erickson E, Wakao S, Niyogi KK. Light stress and photoprotection in *Chlamydomonas reinhardtii*. *Plant J*. 2015:82(3):449–465. https://doi.org/10.1111/tpj.12825

Foyer C, Furbank R, Harbinson J, Horton P. The mechanisms contributing to photosynthetic control of electron transport by carbon assimilation in leaves. *Photosynth Res*. 1990:25(2):83–100. https://doi.org/10.1007/BF00035457

Gargouri M, Bates PD, Park J-J, Kirchhoff H, Gang DR. Functional photosystem I maintains proper energy balance during nitrogen depletion in *Chlamydomonas reinhardtii*, promoting triacylglycerol accumulation. *Biotechnol Biofuels*. 2017:10(1):89. https://doi.org/10.1186/s13068-017-0774-4

Geigenberger P, Fernie AR. Metabolic control of redox and redox control of metabolism in plants. *Antioxid Redox Signal*. 2014:21(9):1389–1421. https://doi.org/10.1089/ars.2014.6018

Geigenberger P, Kolbe A, Tiessen A. Redox regulation of carbon storage and partitioning in response to light and sugars. *J Exp Bot*. 2005:56(416):1469–1479. https://doi.org/10.1093/jxb/eri178

Gerotto C, Alboresi A, Meneghesso A, Jokel M, Suorsa M, Aro E-M, Morosinotto T. Flavodiiron proteins act as safety valve for electrons in Physcomitrella patens. *Proc Natl Acad Sci U S A*. 2016:113(43):12322–12327. https://doi.org/10.1073/pnas.1606685113

Goodenough U, Blaby I, Casero D, Gallaher SD, Goodson C, Johnson S, Lee J-H, Merchant SS, Pellegrini M, Roth R, *et al*. The path to triacylglyceride obesity in the sta6 strain of *Chlamydomonas reinhardtii*. *Eukaryot Cell*. 2014:13(5):591–613. https://doi.org/10.1128/EC.00013-14

Goodson C, Roth R, Wang ZT, Goodenough U. Structural correlates of cytoplasmic and chloroplast lipid body synthesis in *Chlamydomonas reinhardtii* and stimulation of lipid body production with acetate boost. *Eukaryot Cell*. 2011:10(12):1592–1606. https://doi.org/10.1128/EC.05242-11

Hertle AP, Blunder T, Wunder T, Pesaresi P, Pribil M, Armbruster U, Leister D. PGRL1 is the elusive ferredoxin-plastoquinone

reductase in photosynthetic cyclic electron flow. *Mol Cell*. 2013:49(3):511–523. https://doi.org/10.1016/j.molcel.2012.11.030

Johnson X, Alric J. Interaction between starch breakdown, acetate assimilation, and photosynthetic cyclic electron flow in *Chlamydomonas reinhardtii*. *J Biol Chem*. 2012:287(31):26445–26452. https://doi.org/10.1074/jbc.M112.370205

Johnson X, Alric J. Central carbon metabolism and electron transport in *Chlamydomonas reinhardtii*: metabolic constraints for carbon partitioning between oil and starch. *Eukaryot Cell*. 2013:12(6):776–793. https://doi.org/10.1128/EC.00318-12

Johnson X, Steinbeck J, Dent RM, Takahashi H, Richaud P, Ozawa S-I, Houille-Vernes L, Petroutsos D, Rappaport F, Grossman AR, *et al*. Proton gradient regulation 5-mediated cyclic electron flow under ATP- or redox-limited conditions: a study of ΔATPase pgr5 and ΔrbcL pgr5 mutants in the green alga *Chlamydomonas reinhardtii*. *Plant Physiol*. 2014:165(1):438–452. https://doi.org/10.1104/pp.113.233593

Jokel M, Johnson X, Peltier G, Aro E-M, Allahverdiyeva Y. Hunting the main player enabling *Chlamydomonas reinhardtii* growth under fluctuating light. *Plant J*. 2018:94(5):822–835. https://doi.org/10.1111/tpj.13897

Jokel M, Kosourov S, Battchikova N, Tsygankov AA, Aro EM, Allahverdiyeva Y. Chlamydomonas flavodiiron proteins facilitate acclimation to anoxia during Sulfur deprivation. *Plant Cell Physiol*. 2015:56(8):1598–1607. https://doi.org/10.1093/pcp/pcv085

Juergens MT, Deshpande RR, Lucker BF, Park J-J, Wang H, Gargouri M, Holguin FO, Disbrow B, Schaub T, Skepper JN, *et al*. The regulation of photosynthetic structure and function during nitrogen deprivation in *Chlamydomonas reinhardtii*. *Plant Physiol*. 2015:167(2):558–573. https://doi.org/10.1104/pp.114.250530

Kaye Y, Huang W, Clowez S, Saroussi S, Idoine A, Sanz-Luque E, Grossman AR. The mitochondrial alternative oxidase from *Chlamydomonas reinhardtii* enables survival in high light. *J Biol Chem*. 2019:294(4):1380–1395. https://doi.org/10.1074/jbc.RA118.004667

Klughammer C, Schreiber U. An improved method, using saturating light pulses, for the determination of photosystem I quantum yield via P700+-absorbance changes at 830 nm. *Planta*. 1994:192(2):261–268. https://doi.org/10.1007/BF01089043

Kong F, Burlacot A, Liang Y, Légeret B, Alseekh S, Brotman Y, Fernie AR, Krieger-Liszkay A, Beisson F, Peltier G, *et al*. Interorganelle communication: peroxisomal MALATE DEHYDROGENASE2 connects lipid catabolism to photosynthesis through redox coupling in Chlamydomonas. *Plant Cell*. 2018:30(8):1824–1847. https://doi.org/10.1105/tpc.18.00361

Kong F, Yamaoka Y, Ohama T, Lee Y, Li-Beisson Y. Molecular genetic tools and emerging synthetic biology strategies to increase cellular oil content in *Chlamydomonas reinhardtii*. *Plant Cell Physiol*. 2019:60(6):1184–1196. https://doi.org/10.1093/pcp/pcz022

Labun K, Montague TG, Krause M, Torres Cleuren YN, Tjeldnes H, Valen E. CHOPCHOP v3: expanding the CRISPR web toolbox beyond genome editing. *Nucleic Acids Res*. 2019:47(W1):W171–W174. https://doi.org/10.1093/nar/gkz365

LeBauer DS, Treseder KK. Nitrogen limitation of net primary productivity in terrestrial ecosystems is globally distributed. *Ecology*. 2008:89(2):371–379. https://doi.org/10.1890/06-2057.1

Légeret B, Schulz-Raffelt M, Nguyen HM, Auroy P, Beisson F, Peltier G, Blanc G, Li-Beisson Y. Lipidomic and transcriptomic analyses of *Chlamydomonas reinhardtii* under heat stress unveil a direct route for the conversion of membrane lipids into storage lipids. *Plant Cell Environ*. 2016:39(4):834–847. https://doi.org/10.1111/pce.12656

Li X, Moellering ER, Liu B, Johnny C, Fedewa M, Sears BB, Kuo M-H, Benning C. A galactoglycerolipid lipase is required for triacylglycerol accumulation and survival following nitrogen deprivation in *Chlamydomonas reinhardtii*. *Plant Cell*. 2012:24(11):4670–4686. https://doi.org/10.1105/tpc.112.105106

Li-Beisson Y, Thelen JJ, Fedosejevs E, Harwood JL. The lipid biochemistry of eukaryotic algae. *Prog Lipid Res*. 2019:74:31–68. https://doi.org/10.1016/j.plipres.2019.01.003

Malone LA, Proctor MS, Hitchcock A, Hunter CN, Johnson MP. Cytochrome b6f—orchestrator of photosynthetic electron transfer. *Biochim Biophys Acta Bioenerg*. 2021:1862(5):148380. https://doi.org/10.1016/j.bbabio.2021.148380

Maxwell K, Johnson GN. Chlorophyll fluorescence—a practical guide. *J Exp Bot*. 2000:51(345):659–668. https://doi.org/10.1093/jexbot/51.345.659

Michelet L, Zaffagnini M, Morisse S, Sparla F, Pérez-Pérez ME, Francia F, Danon A, Marchand CH, Fermani S, Trost P, *et al*. Redox regulation of the calvin–benson cycle: something old, something new. *Front Plant Sci*. 2013:4:470. https://doi.org/10.3389/fpls.2013.00470

Miller R, Wu G, Deshpande RR, Vieler A, Gärtner K, Li X, Moellering ER, Zäuner S, Cornish AJ, Liu B, *et al*. Changes in transcript abundance in *Chlamydomonas reinhardtii* following nitrogen deprivation predict diversion of metabolism. *Plant Physiol*. 2010:154(4):1737–1752. https://doi.org/10.1104/pp.110.165159

Munekage Y, Hojo M, Meurer J, Endo T, Tasaka M, Shikanai T. PGR5 is involved in cyclic electron flow around photosystem I and is essential for photoprotection in Arabidopsis. *Cell*. 2002:110(3):361–371. https://doi.org/10.1016/S0092-8674(02)00867-X

Munekage Y, Takeda S, Endo T, Jahns P, Hashimoto T, Shikanai T. Cytochrome b6f mutation specifically affects thermal dissipation of absorbed light energy in Arabidopsis. *Plant J*. 2001:28(3):351–359. https://doi.org/10.1046/j.1365-313X.2001.01178.x

Park J-J, Wang H, Gargouri M, Deshpande RR, Skepper JN, Holguin FO, Juergens MT, Shachar-Hill Y, Hicks LM, Gang DR. The response of *Chlamydomonas reinhardtii* to nitrogen deprivation: a systems biology analysis. *Plant J*. 2015:81(4):611–624. https://doi.org/10.1111/tpj.12747

Peers G, Truong TB, Ostendorf E, Busch A, Elrad D, Grossman AR, Hippler M, Niyogi KK. An ancient light-harvesting protein is critical for the regulation of algal photosynthesis. *Nature*. 2009:462(7272):518–521. https://doi.org/10.1038/nature08587

Peltier G, Schmidt GW. Chlororespiration: an adaptation to nitrogen deficiency in *Chlamydomonas reinhardtii*. *Proc Natl Acad Sci U S A*. 1991:88(11):4791–4795. https://doi.org/10.1073/pnas.88.11.4791

Peltier G, Stoffel C, Findinier J, Madireddi SK, Dao O, Epting V, Morin A, Grossman A, Li-Beisson Y, Burlacot A. Alternative electron pathways of photosynthesis power green algal CO2 capture. *Plant Cell*. 2024;36(10):4132–4142. https://doi.org/10.1093/plcell/koae143

Penzler J-F, Marino G, Reiter B, Kleine T, Naranjo B, Leister D. Commonalities and specialties in photosynthetic functions of PROTON GRADIENT REGULATION5 variants in Arabidopsis. *Plant Physiol*. 2022:190(3):1866–1882. https://doi.org/10.1093/plphys/kiac362

Petroutsos D, Terauchi AM, Busch A, Hirschmann I, Merchant SS, Finazzi G, Hippler M. PGRL1 participates in iron-induced remodeling of the photosynthetic apparatus and in energy metabolism in *Chlamydomonas reinhardtii*. *J Biol Chem*. 2009:284(47):32770–32781. https://doi.org/10.1074/jbc.M109.050468

Rühle T, Dann M, Reiter B, Schünemann D, Naranjo B, Penzler J-F, Kleine T, Leister D. PGRL2 triggers degradation of PGR5 in the absence of PGRL1. *Nat Commun*. 2021:12(1):3941. https://doi.org/10.1038/s41467-021-24107-7

Saint-Sorny M, Brzezowski P, Arrivault S, Alric J, Johnson X. Interactions between carbon metabolism and photosynthetic electron transport in a *Chlamydomonas reinhardtii* mutant without CO2 fixation by RuBisCO. *Front Plant Sci*. 2022:13:876439. https://doi.org/10.3389/fpls.2022.876439

Saroussi S, Karns DAJ, Thomas DC, Bloszies C, Fiehn O, Posewitz MC, Grossman AR. Alternative outlets for sustaining photosynthetic electron transport during dark-to-light transitions. *Proc Natl Acad Sci U S A*. 2019:116(23):11518–11527. https://doi.org/10.1073/pnas.1903185116

Saroussi S, Redekop P, Karns DAJ, Thomas DC, Wittkopp TM, Posewitz MC, Grossman AR. Restricting electron flow at cytochrome b6f when downstream electron acceptors are severely limited. *Plant Physiol*. 2023:192(2):789–804. https://doi.org/10.1093/plphys/kiad185

Saroussi S, Sanz-Luque E, Kim RG, Grossman AR. Nutrient scavenging and energy management: acclimation responses in nitrogen and sulfur deprived Chlamydomonas. *Curr Opin Plant Biol*. 2017:39:114–122. https://doi.org/10.1016/j.pbi.2017.06.002

Saroussi SI, Wittkopp TM, Grossman AR. The type II NADPH dehydrogenase facilitates cyclic electron flow, energy-dependent quenching, and chlororespiratory metabolism during acclimation of *Chlamydomonas reinhardtii* to nitrogen deprivation. *Plant Physiol*. 2016:170(4):1975–1988. https://doi.org/10.1104/pp.15.02014

Schmollinger S, Mühlhaus T, Boyle NR, Blaby IK, Casero D, Mettler T, Moseley JL, Kropat J, Sommer F, Strenkert D, *et al*. Nitrogen-Sparing mechanisms in Chlamydomonas affect the transcriptome, the proteome, and photosynthetic metabolism. *Plant Cell*. 2014:26(4):1410–1435. https://doi.org/10.1105/tpc.113.122523

Schulz-Raffelt M, Chochois V, Auroy P, Cuiné S, Billon E, Dauvillée D, Li-Beisson Y, Peltier G. Hyper-accumulation of starch and oil in a Chlamydomonas mutant affected in a plant-specific DYRK kinase. *Biotechnol Biofuels*. 2016:9(1):55. https://doi.org/10.1186/s13068-016-0469-2

Siaut M, Cuiné S, Cagnon C, Fessler B, Nguyen M, Carrier P, Beyly A, Beisson F, Triantaphylidès C, Li-Beisson Y, *et al*. Oil accumulation in the model green alga *Chlamydomonas reinhardtii*: characterization, variability between common laboratory strains and relationship with starch reserves. *BMC Biotechnol*. 2011:11(1):7. https://doi.org/10.1186/1472-6750-11-7

Steinbeck J, Nikolova D, Weingarten R, Johnson X, Richaud P, Peltier G, Hermann M, Magneschi L, Hippler M. Deletion of proton gradient regulation 5 (PGR5) and PGR5-like 1 (PGRL1) proteins promote sustainable light-driven hydrogen production in *Chlamydomonas reinhardtii* due to increased PSII activity under sulfur deprivation. *Front Plant Sci*. 2015:6:892. https://doi.org/10.3389/fpls.2015.00892

Stiehl HH, Witt HT. Quantitative treatment of the function of plastoquinone in phostosynthesis. *Z Naturforsch B*. 1969:24(12):1588–1598. https://doi.org/10.1515/znb-1969-1219

Tagawa K, Tsujimoto HY, Arnon DI. Role of chloroplast ferredoxin in the energy conversion process of photosynthesis. *Proc Natl Acad Sci U S A*. 1963:49(4):567–572. https://doi.org/10.1073/pnas.49.4.567

Takeuchi T, Benning C. Nitrogen-dependent coordination of cell cycle, quiescence and TAG accumulation in Chlamydomonas. *Biotechnol Biofuels*. 2019:12(1):292. https://doi.org/10.1186/s13068-019-1635-0

Tolleter D, Ghysels B, Alric J, Petroutsos D, Tolstygina I, Krawietz D, Happe T, Auroy P, Adriano J-M, Beyly A, *et al*. Control of hydrogen photoproduction by the proton gradient generated by cyclic electron flow in *Chlamydomonas reinhardtii*. *Plant Cell*. 2011:23(7):2619–2630. https://doi.org/10.1105/tpc.111.086876

Tran Q-G, Cho K, Park S-B, Kim U, Lee YJ, Kim H-S. Impairment of starch biosynthesis results in elevated oxidative stress and autophagy activity in *Chlamydomonas reinhardtii*. *Sci Rep*. 2019:9(1):9856. https://doi.org/10.1038/s41598-019-46313-6

Upadhyaya S, Agrawal S, Gorakshakar A, Rao BJ. TOR kinase activity in *Chlamydomonas reinhardtii* is modulated by cellular metabolic states. *FEBS Lett*. 2020:594(19):3122–3141. https://doi.org/10.1002/1873-3468.13888

Vitousek PM, Howarth RW. Nitrogen limitation on land and in the sea: how can it occur? *Biogeochemistry*. 1991:13(2):87–115. https://doi.org/10.1007/BF00002772

Wada S, Yamamoto H, Suzuki Y, Yamori W, Shikanai T, Makino A. Flavodiiron protein substitutes for cyclic electron flow without competing CO2 assimilation in rice. *Plant Physiol*. 2018:176(2):1509–1518. https://doi.org/10.1104/pp.17.01335

Wu S, Gu W, Huang A, Li Y, Kumar M, Lim PE, Huan L, Gao S, Wang G. Elevated CO2 improves both lipid accumulation and growth rate in the glucose-6-phosphate dehydrogenase engineered phaeodactylum tricornutum. *Microb Cell Fact*. 2019:18(1):161. https://doi.org/10.1186/s12934-019-1214-x

Yamamoto H, Shikanai T. PGR5-Dependent cyclic electron flow protects photosystem I under fluctuating light at donor and acceptor sides. *Plant Physiol*. 2019:179(2):588–600. https://doi.org/10.1104/pp.18.01343

Zhang Y-M, Chen H, He C-L, Wang Q. Nitrogen starvation induced oxidative stress in an oil-producing green alga chlorella sorokiniana C3. *PLoS One*. 2013:8(7):e69225. https://doi.org/10.1371/journal.pone.0069225

Zhou Q, Yamamoto H, Shikanai T. Distinct contribution of two cyclic electron transport pathways to P700 oxidation. *Plant Physiol*. 2023:192(1):326–341. https://doi.org/10.1093/plphys/kiac557

Zienkiewicz K, Du Z-Y, Ma W, Vollheyde K, Benning C. Stress-induced neutral lipid biosynthesis in microalgae—molecular, cellular and physiological insights. *Biochim Biophys Acta*. 2016:1861(9):1269–1281. https://doi.org/10.1016/j.bbalip.2016.02.008